Optical and Quantum Electronics **36:** 681–697, 2004.
© 2004 *Kluwer Academic Publishers. Printed in the Netherlands.*

Review

Modelling laser-based table-top THz sources: Optical rectification, propagation and electro-optic sampling

J. FAURE[1 * †], J. VAN TILBORG[2 ‡], R. A. KAINDL[2] AND W. P. LEEMANS[2]
[1]*Laboratoire d'Optique Appliquée, ENSTA-Ecole Polytechnique, UMR 7639, 91761 Palaiseau, France;*
[2]*E. O. Lawrence Berkeley National Laboratory, University of California, Berkeley 94720, USA*
*(*author for correspondence: E-mail: jfaure@ensta.fr)*

Received 21 April 2004; accepted 7 May 2004

Abstract. A model describing the generation of THz pulses by optical rectification and the detection of THz pulses by electro-optic sampling is presented. The model is comprehensive and mostly analytical: physical phenomena such as dispersion, group velocity mismatch, multiple reflections and diffraction are represented by one dimensional transfer functions. The model is compared with experimental results and shows good agreement with experiments. It is shown that including diffraction is crucial for retrieving the details of the THz spectrum.

Key words. electro-optic sampling, optical rectification, diffraction, THz radiation, transfer function, ultra-short laser pulses

1. Introduction

The generation and detection of THz electromagnetic sources has been a growing field of research in the past decade (Grischkowsky 2003). This is due to the numerous applications these sources can offer, such as biological imaging with THz pulses (Wu *et al.* 1996; Mittleman *et al.* 1999; Beard *et al.* 2002), object reconstruction with single-cycle THz pulses (Ruffin*et al.* 2001), time-resolved spectroscopy for solid-state physics and material science in the mid-infrared region (Auston and Cheung 1984; Grischkowsky *et al.* 1990; Katzenellenbogen *et al.* 1992; Jeon and Grischkowsky 1998; Kaindl *et al.* 1998; 2003; Elsaesser and Woerner 1999; Huber *et al.* 2001). This frequency range is of particular interest since it covers vibrational and electronic resonances of important molecular systems as well as solids. THz fields can be generated in many different ways. For instance, coherent synchrotron

[†]Previously at Lawrence Berkeley National Laboratory.
[‡]Also at Technische Universiteit Eindhoven, the Netherlands.

radiation from accelerators can produce high average powers in the THz range (Carr *et al.* 2002; Williams *et al.* 2002), and recently, a novel method using laser driven accelerators has been proposed to produce high peak power THz fields (Leemans *et al.* 2003). Another more compact alternative is to use ultrafast lasers in conjunction with high-speed photoconductors which are used as transient current sources for radiative antennas (Auston *et al.* 1984b; Ralph and Grischkowsky 1992). However, much higher frequencies have been obtained with nonlinear optical rectification (Bass *et al.* 1962) of ultra-short lasers in dielectric crystals or semiconductors (Xu *et al.* 1992; Zhang *et al.* 1992; Rice *et al.* 1994). On the detection side, very large detection bandwidths have been obtained by using electro-optic sampling (Valdmanis *et al.* 1982) in nonlinear crystals (Wu and Zhang 1995; Nahata *et al.* 1996). Both methods are based on frequency mixing in nonlinear materials and seem to offer good performance and flexibility. Experimental set-ups based on optical rectification and electro-optic sampling can result in a variety of THz sources, ranging from single cycle THz pulses (Xu *et al.* 1992), narrowband sources in periodical media (Lee *et al.* 2000) to ultra-broadband mid-infrared pulses (Bonvalet *et al.* 1995). Recently, the use of very short laser pulses (< 20 fs) and very thin crystals ($< 30\,\mu$m) have allowed the generation and detection of THz radiation extending into the mid-infrared, with frequencies from 0.1 to 70 THz (Bonvalet *et al.* 1995; Bakker *et al.* 1998; Han and Zhang 1998; Kaindl *et al.* 1999; Huber *et al.* 2000).

In this paper, we present a general and comprehensive model for describing THz sources based on optical rectification and electro-optic sampling. The model is mostly analytical and relevant physical phenomena are represented by one dimensional transfer functions. Fig. 1 shows a schematic of a typical laser-based THz source: first, a short pulse generates a THz transient in a nonlinear generation crystal. Then, the THz pulse has to propagate from the generation crystal to the detection crystal through the imaging optics. More often than not, filters are introduced in the beam path in order to separate the laser light from the THz field. The THz beam can be focused onto a sample

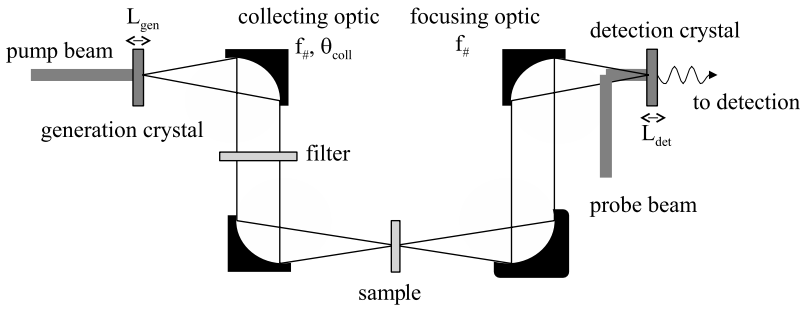

Fig. 1. Schematic of a typical table-top THz source. L_{gen} and L_{det} are the generation and detection crystal lengths, respectively.

to be studied, and then again collected before being mixed with a probe laser pulse inside the detection crystal. Considerable work has already been devoted to modelling the detection part of this problem (Bakker *et al.* 1998; Gallot and Grischkowsky 1999; Leitenstorfer *et al.* 1999). Here, we will present a model that encompasses the full set-up: in Section 2, we derive an expression for the THz field inside the generation crystal. In Section 3, the propagation of the THz field through the imaging system is discussed and we introduce transfer functions for modelling diffraction, focusing of the THz beam, and other effects. In Section 4, we introduce a transfer function for the detection crystal and finally, in Section 5, we compare the results of our model to experiments.

2. Optical rectification of sub-picosecond laser pulses

Optical rectification (Bass *et al.* 1962) is a second order nonlinear effect corresponding to the generation of low-frequency radiation by frequency difference. Physically, optical rectification is the low-frequency response of a nonlinear material to the envelope of a short and intense laser pulse. Mathematically, the problem can be described by the following equations:

$$\left(\nabla^2 - \frac{\epsilon(\omega)}{c^2}\frac{\partial^2}{\partial \mathrm{T}^2}\right)\mathbf{E}_{\mathrm{THz}}(z,t) = \frac{4\pi}{c^2}\frac{\partial^2 \mathbf{P}_{\mathrm{NL}}(z,t)}{\partial t^2,} \tag{1}$$

$$P^i_{\mathrm{NL}}(\omega) = \int_{-\infty}^{+\infty} \sum_{j,k} \chi^{(2)}_{ijk}(\omega;\omega_0,-\omega_0+\omega)E^j_L(\omega_0)E^k_L(\omega_0-\omega)\,\mathrm{d}\omega_0, \tag{2}$$

where ω_0 is the central frequency of the laser field, $\omega \ll \omega_0$ is the frequency of the THz field, E_{THz} is the THz field generated by the nonlinearity, $\epsilon(\omega)$ is the dielectric function, P_{NL} is the nonlinear polarization of the medium (at low frequency) and E_{L} is the high-intensity laser field causing the nonlinearity (itself a solution of similar wave equations).

Solving these equations is not trivial, but several simplifications can be made to make the problem more tractable. The two main physical effects which should be taken into account are the following: (i) dispersion and absorption of the THz field, (ii) phase mismatch between the laser pulse and the THz pulse. If the Rayleigh lengths of both THz and laser fields are longer than the crystal thickness, one can reduce Equation (1) to a one-dimensional equation. This assumption should hold true for most practical systems: in a well designed system, the Rayleigh length of the laser beam should be longer than the crystal length in order to benefit from the high laser intensity throughout the whole crystal. Although this assumption might break down

for the far-infrared, typically below 1 THz, these very low frequencies are greatly suppressed by diffraction, as will be discussed in Section 3. In addition, the geometry of the fields with respect to the crystal axes in Equation (2) can be modeled simply by using an effective nonlinear coefficient $\chi^{(2)}_{\text{eff}}(\theta, \phi, \omega)$, denoted as $\chi^{(2)}(\omega)$ in what follows. In this case, assuming a non resonant nonlinearity, Equations (1) and (2) reduce to the following 1D equation:

$$\left(\frac{\partial^2}{\partial z^2} - \frac{\epsilon(\omega)}{c^2}\frac{\partial^2}{\partial t^2}\right) E_{\text{THz}}(z,t) = \frac{4\pi}{c^2}\chi^{(2)}(\omega)\frac{\partial^2}{\partial t^2}\left|E_{\text{L}}(z,t)\right|^2. \tag{3}$$

For the laser field, we neglect pump depletion as well as absorption (see note 1 for details), and assume the envelope to be Gaussian:

$$E_{\text{L}}(z,t) = \frac{E_0}{2}\exp\left[-\frac{(t - z/v_{\text{g}})^2}{2\tau(z)^2}\right]\exp[-\text{i}(\omega_0 t - k_0 z)] + c.c., \tag{4}$$

where $v_{\text{g}} = (\partial\omega/\partial k)_{\omega_0}$ is the group velocity of the laser pulse and τ is the pulse duration at $1/e$ in intensity ($\tau_{\text{FWHM}} = 2\sqrt{\ln 2}\tau$). In general, the laser pulse stretches due to dispersion through the material, and τ is a function of z. Assuming that the main contribution to dispersion is the second-order term in the phase, the laser pulse duration then evolves as $\tau(z) = \tau_0$ c$[1 + z^2/z_{\text{D}}^2]^{1/2}$, where τ_0 is the transform limited pulse duration and $z_{\text{D}} = \tau_0^2 v_{\text{g}}^2/(4\ \ln 2\, \partial\ v_{\text{g}}/\partial\omega)$ is the distance it takes for the pulse to stretch by $\sqrt{2}$. In most practical cases, the crystal length is smaller than this dispersion length and in the following, we will consider that the laser pulse has a fixed pulse duration τ which does not evolve during propagation in the generation crystal.

The problem can now be treated analytically by taking the Fourier transform of Equation (3) and using Equation (4):

$$\left(\frac{\partial^2}{\partial z^2} + \omega^2\frac{\epsilon(\omega)}{c^2}\right) E_{\text{THz}}(z,\omega) = -\frac{\sqrt{2}\pi\omega^2\chi^{(2)}(\omega)}{c^2}\tau\exp\left[-\frac{\omega^2\tau^2}{4}\right]\exp[\text{i}\omega z/v_{\text{g}}]E_0^2. \tag{5}$$

This equation can be solved using the following set of boundary conditions: $E_{\text{THz}}(z=0,\omega) = 0$ and $\frac{\partial}{\partial z}E_{\text{THz}}(z=0,\omega) = 0$. The solution is

$$\begin{aligned} E_{\text{THz}}(z,\omega) = \frac{\sqrt{2}\pi\chi^{(2)}(\omega)}{n_{\text{THz}}^2 - n_{\text{g}}^2}\tau\exp\left[-\frac{\omega^2\tau^2}{4}\right]E_0^2\Bigg[\frac{1}{2}\left(1 + \frac{n_{\text{g}}}{n_{\text{THz}}}\right)\exp^{(\text{i}\omega n_{\text{THz}} z/c)} \\ + \frac{1}{2}\left(1 - \frac{n_{\text{g}}}{n_{\text{THz}}}\right)\exp^{(-\text{i}\omega n_{\text{THz}} z/c)} - \exp^{(\text{i}\omega n_{\text{g}} z/c)}\Bigg] \end{aligned} \tag{6}$$

where n_g is the laser group index defined as $n_g = c/v_g$, $n_{THz}(\omega) = \sqrt{\epsilon(\omega)} = n + i\kappa$ is the complex index of refraction of the material in the infrared spectral range; n is the real index of refraction and κ is the absorption coefficient. It should be noted that in this last expression, both n_{THz} and $\chi^{(2)}$ are functions of ω, accounting for dispersion, absorption of the THz pulse, as well as for the frequency dependent nonlinearity (see Appendix). According to Equation (6), the resulting THz field is the sum of three terms: the first term is forward propagating with phase velocity $v_{THz} = c/n_{THz}$, the second term is backward propagating at v_{THz} but it has a lower amplitude and can be neglected. The third term is also forward propagating but with phase velocity c/n_g. Interference between these three terms will result in the creation of the THz waveform. Another interesting point is the term $\exp(-\omega^2\tau^2/4)$, which acts as a spectral filter. It illustrates the expected result that shorter laser pulse durations permit the generation of higher THz frequencies. In general, Equation (6) is then numerically inverse Fourier transformed in order to provide the shape of the THz field in the time domain. Neglecting dispersion, one can obtain an analytical estimate of the THz field shape (similar to the result of Xu *et al.* 1992),

$$E_{THz}(z,t) \propto \left\{ \frac{1}{2}\left(1+\frac{n_g}{n_{THz}}\right)\exp\left[-\frac{(t-z/v_{THz})^2}{\tau^2}\right] + \frac{1}{2}\left(1-\frac{n_g}{n_{THz}}\right)\exp\left[-\frac{(t+z/v_{THz})^2}{\tau^2}\right] - \exp\left[-\frac{(t-z/v_g)^2}{\tau^2}\right] \right\}. \quad (7)$$

However, this expression is not of much practical use since dispersion cannot be neglected for the THz fields generated through optical rectification of subpicosecond pulses, as they are generally broadband. This limits the usefulness of Equation (7) to optical rectification of pulses which are a few picoseconds long. To illustrate the validity range of Equation (7), Fig. 2 shows a comparison between the numerical inverse Fourier transform of Equation (6) and the results of Equation (7). As seen in Fig. 2(a), the agreement between the two expressions is excellent for laser pulse lengths longer than 2 ps. However, the analytical expression severely fails for 100 fs pulses, as seen in Fig. 2(b). These calculations were done assuming a 500 μm thick crystal and a laser with central wavelength $\lambda_0 = 800$ nm.

3. Propagation effects

We now focus on the propagation of the THz field from the generation crystal to the detection crystal. First, the THz pulse has to exit the generation

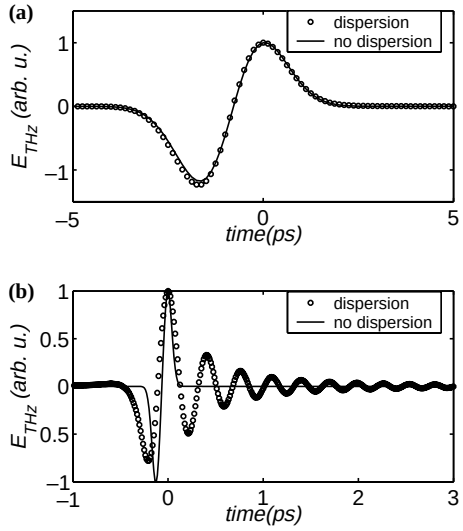

Fig. 2. Comparison between the waveform obtained with analytical expression from Equation (7) (solid line) and the inverse Fourier transform of Equation (6) (circles). (a) Optical rectification in a 500 μm long ZnTe crystal using a laser pulse with duration 2 ps (FWHM) and central wavelength 800 nm. (b) Same parameters with a 100 fs pulse.

crystal; it also has to enter the detection crystal. At each interface, the pulse undergoes frequency-dependent reflections and transmissions. If the round-trip travel time inside the crystal is shorter than the THz pulse length, then the THz pulse can undergo multiple reflections, giving rise to a Fabry–Perot effect. All of these effects are linear and can be very easily modelled by transfer functions. At the vacuum-crystal interface, the reflection and transmission coefficients for the electric field are the well-known Fresnel coefficients: $R_{\mathrm{in}}(\omega) = (\sqrt{\epsilon} - 1)/(\sqrt{\epsilon} + 1)$ and $T_{in}(\omega) = 2/(\sqrt{\epsilon} + 1)$. At the crystal–vacuum interface, the coefficients are: $R_{\mathrm{out}}(\omega) = (1 - \sqrt{\epsilon})/(1 + \sqrt{\epsilon})$ and $T_{\mathrm{out}}(\omega) = 2\sqrt{\epsilon}/(\sqrt{\epsilon} + 1)$. Here, the THz pulse was assumed to penetrate the crystal at normal incidence; the case of arbitrary incidence is polarization dependent and can easily be found in the literature (Jackson 1962).

The transfer function for the Fabry–Perot effect is simply given by

$$T_{\mathrm{FP}}(L, \omega) = \frac{1}{1 + R_{\mathrm{out}}^2 \exp\left[2\mathrm{i}n_{\mathrm{THz}}\omega L/c\right]}, \tag{8}$$

where L is the length of the crystal. Usually, a piece of material will be introduced in the path of the THz pulse, such as a filter which transmits the THz field and blocks the pump laser light, or a sample that will be studied. The THz field will then undergo dispersion, absorption and distortion in the sample. These linear effects can be described by the following transfer function:

$$T_{\text{filter}}(\omega, L) = \frac{T_{\text{in}} T_{\text{out}}}{1 + R_{\text{out}}^2 \exp\left[2\text{i}n_{\text{THz}}\omega L/c\right]} \exp\left[\text{i}n_{\text{THz}}\omega L/c\right]. \tag{9}$$

A more delicate issue is diffraction: the THz field usually originates from a small source point. It will diffract out and be collected by the first collecting optics. As was observed in a recent experiment (Xu and Zhang 2002), the efficiency of collection is a very strong function of wavelength. In particular the low frequency part of the spectrum diffracts out very quickly and the efficiency of the collection to the far field, where the detection actually occurs, is very weak for these low frequencies. The goal of the following discussion is not to provide a full description of diffraction (as was done in a recent publication (Côté *et al.* 2003)), but rather to find analytical approximate transfer functions that describe the phenomena at stake reasonably well.

An incident Gaussian laser beam with radius r_{L} at $1/e^2$ in intensity will generate a THz beam which is also Gaussian, but with radius $r_0 = r_{\text{L}}/\sqrt{2}$. When the wavelength of the radiation is small compared to r_0, $kr_0 \gg 1$, the paraxial approximation holds and the propagation can be described by Gaussian optics. In this case, the radius of the beam evolves as $\sigma(z) = r_0(1 + z^2/z_{\text{R}}^2)^{1/2} \simeq r_0 z/z_{\text{R}}$ for $z \gg z_{\text{R}}$, where $z_{\text{R}} = kr_0^2/2$ is the Rayleigh length of the THz beam. For a collecting optic with diameter D placed at distance l from the generation crystal, the transfer function for the electric field is given by

$$T_{\text{parax}}(\omega) = \left[\frac{\int_0^{D/2} \exp\left[-r^2/\sigma(l)^2\right] r \, \text{d}r}{\int_0^{+\infty} \exp\left[-r^2/\sigma(l)^2\right] r \, \text{d}r}\right]^{1/2}. \tag{10}$$

However, the paraxial approximation does not hold for low frequencies and such a description of the beam propagation is invalid. In the limit where $kr_0 \ll 1$, one can use Bethe's diffraction theory (Bethe 1944) to describe the propagation of the THz beam (see note 2). In this regime, the typical diffraction length, analogous to the Rayleigh length in Gaussian optics, is given by $z_{\text{B}} = k^2 r_0^3/2$. This shows that low frequencies diffract much quicker than predicted by the paraxial approximation. The transfer function for diffraction can be calculated from Bethe's result and from Equation (10):

$$T_{\text{diff}}(\omega) = \begin{cases} \left(1 - \exp\left[-\frac{\tan^2(\theta_{\text{coll}}) k^2 r_0^2}{4}\right]\right)^{1/2} & \text{for } kr_0 > 1 \text{ (paraxial)}, \\ \frac{2\sqrt{2} k^2 r_0^2}{3\pi}\left(\frac{8}{3} - \frac{5\cos(\theta_{\text{coll}})}{2} - \frac{\cos(3\theta_{\text{coll}})}{6}\right)^{1/2} & \text{for } kr_0 < 1 \text{ (Bethe)}, \end{cases} \tag{11}$$

where θ_{coll} is the half collection angle: $\theta_{\text{coll}} = \arctan[D/(2f_{\text{coll}})] = \arctan[1/(2f_{\#})]$. Here $f_{\#}$ is the f-number of the collection optics. For simplicity,

one can simply develop Equation (10) and use the heuristic transfer function defined as

$$T_{\mathrm{diff}}(\omega) = \left(1 - \exp\left[-\frac{\tan^2(\theta_{\mathrm{coll}}) z_{\mathrm{diff}}^2}{r_0^2}\right]\right)^{1/2}, \tag{12}$$

where the diffraction distance is $z_{\mathrm{diff}} = z_{\mathrm{R}}$ for $kr_0 > 1$ and $z_{\mathrm{diff}} = z_{\mathrm{B}}$ for $kr_0 < 1$. In Fig. 3 we present a comparison of the two different diffraction transfer functions: the one given by Equation (11) (dash-dotted line) and the heuristic one given by Equation (12). The agreement between the two expressions is excellent whether the source size is 300 μm, as in Fig. 3(a), or 30 μm, as in Fig. 3(b). Fig. 3 also illustrates the sharp cut-off that diffraction causes for THz wavelengths smaller than the source size.

Finally, the last point concerns the focusing of the THz field: as was discussed before, the propagation of the THz beam depends strongly on the frequency. This will impact the focusing of the beam: different frequencies will be focused to different spot sizes which also changes the strength of the electric field as a function of frequency. First, one has to compute the size of the beam at the last focusing optics of the set-up. For a set-up resembling the one in Fig. 1, the size of the beam at the last focusing optics can be approximated by

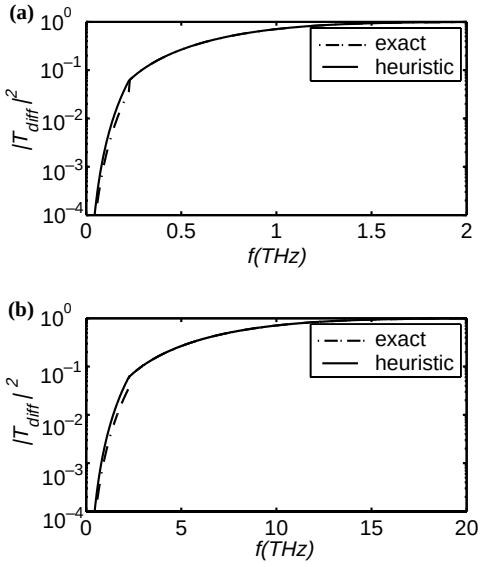

Fig. 3. Transfer function for diffraction $|T_{\mathrm{diff}}|^2$ given by Equation (11) (dash-dotted line) and given by the heuristic formula from Equation (12) (full line). (a) The THz source size is $r_0 = 300\,\mu\mathrm{m}$ and the f-number of the collecting optic is $f_{\#} = 1$. (b) Same parameters with a source size of $r_0 = 30\,\mu\mathrm{m}$.

$$r_{\text{in}}(\omega) = \min\left[\frac{D}{2}, r_0\left(1 + \frac{f_{\text{coll}}^2}{z_{\text{diff}}(\omega)^2}\right)^{1/2}\right], \tag{13}$$

where f_{coll} is the focal length of the collecting optics and D is its diameter. The size of the beam focused onto the detection crystal is then (assuming Gaussian optics)

$$r_{\text{foc}}(\omega) = \frac{2cf_{\text{foc}}}{\omega r_{\text{in}}(\omega)}. \tag{14}$$

The transfer function for beam focusing is then simply given by

$$T_{\text{focus}}(\omega) = \frac{r_{\text{in}}(\omega)}{r_{\text{foc}}(\omega)}. \tag{15}$$

In conclusion, we have modelled all linear propagation effects occurring in the transport of the THz pulse from the generation crystal to the detection crystal using 1D transfer functions. The field at the input of the detection crystal can be inferred by calculating the following:

$$E_{\text{THz}}^{\text{input}}(\omega) = T_{\text{propag}}(\omega)E_{\text{THz}}(L_{\text{gen}}, \omega), \tag{16}$$

$$T_{\text{propag}}(\omega) = T_{\text{out}}T_{\text{FP}}T_{\text{filter}}T_{\text{diff}}T_{\text{focus}}, \tag{17}$$

where L_{gen} is the length of the generation crystal. The expressions for $E_{\text{THz}}(L_{\text{gen}}, \omega)$ and all the transfer functions are given by Equations (6)–(15). By inverse Fourier transform, the temporal waveform of the THz field at the input of the detection crystal can be computed. As an example, Fig. 4 illustrates some of these propagation effects. The parameters have been chosen so as to demonstrate the dramatic effect that diffraction can have on low frequencies: Fig. 4(a) represents the THz waveform generated inside a 10 μm thick ZnTe crystal by a 20 fs laser pulse at 800 nm and focused to a spot size with radius $r_{\text{L}} = 20\,\mu\text{m}$. Fig. 4(b) represents the same waveform after exiting the generation crystal and after diffracting out in a $f_{\#} = 1$ collection cone. One can notice the emergence of low amplitude replicas of the main waveform; this is due to multiple reflections in the crystal. The difference between the two cases is quite clear in Fig. 4(c) where the spectra before (solid line) and after propagation (dashed line) are shown: frequencies below 5 THz have been strongly attenuated by diffraction. In addition, the spectrum above 5 THz is strongly modulated by the Fabry–Perot effect (see note 3).

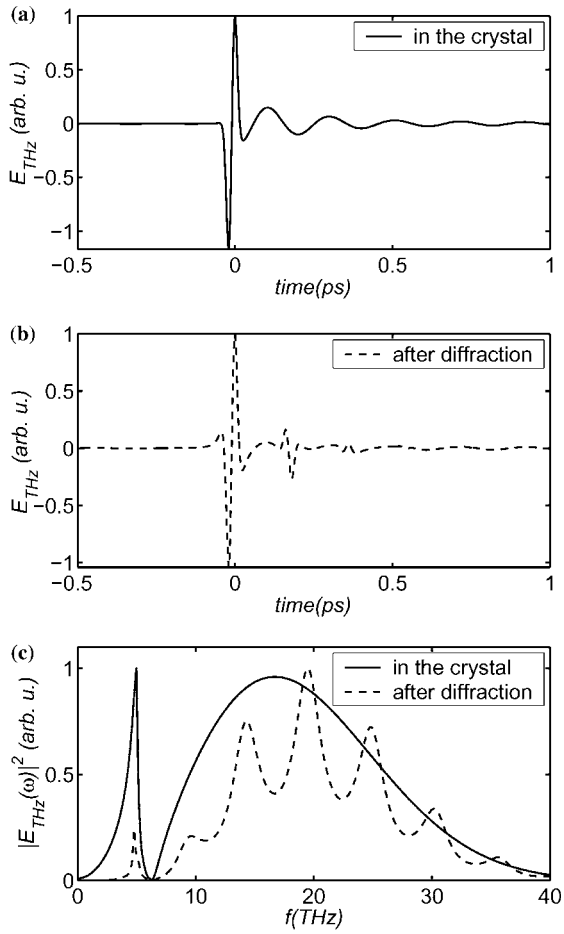

Fig. 4. Illustration of some propagation effects on the THz waveform. (a) THz waveform generated inside a 10 μm thick ZnTe crystal by a 20 fs laser pulse at 800 nm and focused to a spot size with radius $r_L = 20\,\mu m$. (b) Same configuration, but the pulse has propagated out of the crystal, has diffracted out and has been collected with a $f_{\#} = 1$ optic. (c) Comparison of the spectra from case a) (solid line) and case b) (dashed line); the strong absorption around 5.5 THz is due to the phonon line in ZnTe. The low frequencies are strongly attenuated after diffraction and the modulation in the spectrum of the (b) case is due to the Fabry–Perot effect.

4. Electro-optic sampling

Electro-optic sampling of THz pulses has been extensively studied in recent years, both experimentally (Wu *et al.* 1995; Nahata *et al.* 1996) and theoretically (Bakker *et al.* 1998; Gallot and Grischkowsky *et al.* 1999; Leitenstorfer *et al.* 1999). Physically, it is similar to optical rectification and can be described with nearly identical equations. Equations (1) and (2) can be used with the exception that it is now a low-frequency field (THz) which mixes with the laser field, instead of the frequency difference of two laser fields

(we now use $\chi^{(2)}(\omega_0;\omega,\omega_0-\omega)$ in Equation (2)). The main effects that must be taken into account are therefore similar: (i) dispersion and absorption of the THz field, (ii) phase mismatch between the laser probe pulse and the THz pulse, (iii) effect of the probe pulse duration on the resolution of the measurement, (iv) transmission at the vacuum-crystal interface and Fabry–Perot effect. This last point has already been addressed in the previous section. Here, we again assume that pump depletion of the laser field can be neglected and that diffraction of the different fields inside the crystal is small. Within the framework of the previous approximations, we now use the main result of the detailed study of (Gallot and Grischkowsky 1999): the slowly varying envelope approximation can be used for the laser pulse (meaning the bandwidth of the pulse is much smaller than the central frequency $\Delta\omega \ll \omega_0$), and the expression for the electro-optic signal is

$$S_{\mathrm{EO}}(t') \propto \int_{-\infty}^{+\infty} \chi^{(2)}(\omega)\,\frac{\exp\left[\mathrm{i}\Delta k(\omega)L_{\mathrm{det}}\right]-1}{\mathrm{i}\Delta k(\omega)}\,E_{\mathrm{THz}}^{\mathrm{input}}(\omega)C_{\mathrm{opt}}(\omega)\exp\left[-\mathrm{i}\omega t'\right]\mathrm{d}\omega, \tag{18}$$

where t' is the time difference between the THz field and the laser probe pulse, L_{det} is the length of the detection crystal, $\Delta k(\omega) = -k_0(\omega_0-\omega) + k_0(\omega_0) + k(\omega)$ is the phase mismatch between the laser field (wave vector $k_0(\omega_0)$), the THz field (wave vector $k(\omega)$) and the difference frequency field (wave vector $k_0(\omega_0-\omega)$). The function C_{opt} is defined as

$$C_{\mathrm{opt}}(\omega) = \int_{-\infty}^{+\infty} E_{\mathrm{p}}^{*}(\Omega-\omega_0)E_{\mathrm{p}}(\Omega-\omega_0-\omega)\,\mathrm{d}\Omega, \tag{19}$$

where E_{p} is the laser probe beam electric field.
In our case, Equations (18) and (19) can be reduced, and taking into account the transmission at the entrance of the crystal as well as the Fabry–Perot effect, one gets the following expression for the transfer function of the detection crystal:

$$T_{\mathrm{det}}(L_{\mathrm{det}},\omega) = T_{\mathrm{in}}T_{\mathrm{FP}}\,\frac{\exp\left[\mathrm{i}L_{\mathrm{det}}(n_{\mathrm{THz}}-n_{\mathrm{g}})\omega/c\right]-1}{\mathrm{i}\omega/c(n_{\mathrm{THz}}-n_{\mathrm{g}})}\exp\left[-\tau_{\mathrm{p}}^2\omega^2/4\right], \tag{20}$$

where τ_{p} is the pulse duration of the probe beam. The first exponential term accounts for dispersion, absorption and phase mismatch while the second exponential term accounts for the loss of resolution caused by the finite duration of the probe beam.

Another important point which will affect the electro-optic signal is related to the geometrical overlap of the probe beam with the THz beam. As was

mentioned earlier, the different frequency components of the THz pulse are focused to different spot sizes. As a consequence, the overlap between the probe beam and the THz beam is also a function of frequency. Following Equation (18), the electro-optic signal can be expressed as a function of radius by

$$S_{\mathrm{EO}}(r,\omega) \propto T_{\mathrm{det}}(\omega) \times \mid E_0(r) \mid^2 E_{\mathrm{THz}}^{\mathrm{input}}(r,\omega), \tag{21}$$

where $E_0(r)$ is the radial profile of the probe beam. We now assume that the probe pulse is Gaussian with radius r_{p} at $1/e^2$, and that the THz pulse is also Gaussian. For each frequency component of the THz pulse, the radius is $r_{\mathrm{foc}}(\omega)$. Assuming that all of the probe pulse is collected for the measurement, one has to integrate Equation (21) in order to compute the total measured electro-optic signal. Thus, the transfer function for this overlapping effect can be described by

$$T_{\mathrm{overlap}}(\omega) = \frac{r_{\mathrm{foc}}(\omega)^2}{\left(2r_{\mathrm{foc}}(\omega)^2 + r_{\mathrm{p}}^2\right)^{1/2}}. \tag{22}$$

In practice, this effect can be important because in experimental set-ups, the probe beam size is usually smaller than the THz beam size. It is interesting to note that the effect of beam focusing (see transfer function T_{focus}) compensates the effect of the beam overlap when the probe beam size is much larger than the THz beam size.

In conclusion, the generation, propagation and detection of THz pulses can be modeled by the following expression:

$$S_{\mathrm{EO}}(\omega) = T_{\mathrm{propag}}(L_{\mathrm{gen}}, \theta_{\mathrm{coll}}, L_{\mathrm{filter}}, f_{\#}) T_{\mathrm{overlap}} T_{\mathrm{det}}(L_{\mathrm{det}}) E_{\mathrm{THz}}(L_{\mathrm{gen}}, \omega). \tag{23}$$

The waveform obtained through electro-optic sampling can be retrieved by inverse Fourier transform of the last expression.

5. Comparison with experiments

In this section, we concentrate on testing our model against experimental results. The experiment was performed using 500 μm thick ⟨110⟩ ZnTe crystals for detection and generation. The laser central wavelength was 805 nm, duration 150 ± 20 fs, spot size 300 μm at FWHM for the generation beam and 160 μm for the probe beam. The collection and focusing optics had f-number 1.2 and 2, respectively. The simulations were performed using the exact same parameters. It is important to note that there was no free parameter in our

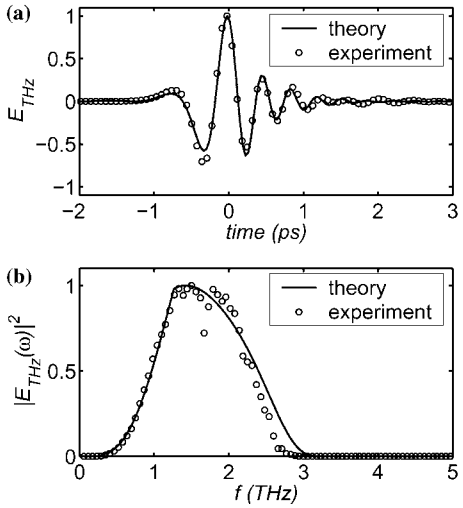

Fig. 5. (a) Comparison between an experimental waveform (circles) and a simulated waveform (full line). (b) Comparison between the corresponding experimental and simulated spectra. The experimental parameters are $\lambda_0 = 805\,\text{nm}$, $\tau_{\text{FWHM}} = 150 \pm 20\,\text{fs}$, $r_0 = 180\,\mu\text{m}$, (corresponding to a laser spot size of $r_{\text{FWHM}} = 300\,\mu\text{m}$ for the pump and $r_{\text{FWHM}} = 160\,\mu\text{m}$ for the probe). The f-number of the collecting optic is $f_{\#} = 1.2$. Both generation and detection crystals are ZnTe and 500 μm thick.

calculations, only the pulse duration was allowed to be changed by the experimental error, which is ± 20 fs. The comparison between experiment and simulation is shown in Fig. 5. Fig. 5(a) shows the measured THz electric field (circles) and the calculation (full line); even small details are reproduced by the simulation. Fig. 5(b) shows the comparison of experimental and simulated spectrum. Here again, the agreement is excellent. The dip in the experimental spectrum around 1.7 THz is due to an absorption line in air. Including diffraction (e.g. including T_{diff}, T_{focus} and T_{overlap} in the calculation) was crucial for retrieving the details of the THz waveform and spectra. When diffraction was not included, it was impossible to obtain simultaneously the correct central wavelength and bandwidth of the THz radiation.

It should be noted that the simulated results are very sensitive to the coefficients of the dielectric function (see Appendix for more details). The results presented in Fig. 5 have been calculated using work by (Gallot *et al.* 1999b) for the coefficients of the dielectric function of ZnTe. For these particular coefficients, the best fit experiment/theory was found using a laser pulse duration of 140 fs, well within the range of experimental errors.

6. Conclusion

We have developed a comprehensive model for describing laser-based THz table-top sources. The model describes the generation of the THz field by

optical rectification of short laser pulses inside the generation crystal. It includes various propagation effects, such as diffraction, dispersion and reflections in the form of simple 1D transfer functions. Finally, the electro-optic detection of the THz field is also expressed as a transfer function. The model was tested and compared with experimental results and showed good quantitative agreement. This validates the numerous approximations which were made in order to keep the model simple. In light of the increasing popularity of laser-based THz sources and their applications, we hope this work will be useful to experimentalists who wish to design or optimize their own THz source.

Acknowledgments

We acknowledge fruitful discussions on diffraction with Carl Schroeder and Gwenael Fubiani.

Appendix: Modeling $\epsilon(\omega)$ and $\chi^{(2)}(\omega)$

The dielectric function in the THz frequency domain can generally be described by the following expression (Bakker *et al.* 1998; Gallot *et al.* 1999b)

$$\epsilon = \epsilon_{\mathrm{el}} + \frac{\epsilon_{\mathrm{st}}\omega_{\mathrm{TO}}^2}{\omega_{\mathrm{TO}}^2 - \omega^2 + 2\mathrm{i}\gamma\omega}. \tag{24}$$

In Table 1, we present the coefficients of two commonly used materials: GaAs and ZnTe. The dielectric function of GaSe in the mid-infrared can be found in (Vodopyanov and Kulevskii 1995). In order to compute the group velocity of the laser pulse, the dielectric function in the visible should also be known. For ZnTe, we used the following function (Marple 1964)

$$n(\lambda) = 4.27 + 3.01 \times \frac{\lambda^2}{\lambda^2 - 0.142}, \tag{25}$$

where λ is in μm. This gives an index of refraction of $n(\lambda = 800\,\mathrm{nm}) = 2.85$, and a group index $n_{\mathrm{g}}(800\,\mathrm{nm}) = 3.24$.

Table 1. Coefficients of the dielectric function in the THz frequency domain for different materials

Material	ϵ_{el}	ϵ_{st}	$\omega_{\mathrm{TO}}/2\pi$ (THz)	γ (THz)	Source
ZnTe	6	3.92	5.32	1	Bakker *et al.* (1998)
ZnTe	7.44	2.58	5.32	<0.157	Gallot *et al.* (1999b)
GaAs	11	2	8	0.5	See note 4

The frequency-dependent nonlinearity is simply modelled using Miller's rule (Miller 1964; Boyd and Pollack 1973): for noncentrosymmetric media, the nonlinearity can be expressed as

$$\chi^{(2)}(\omega;\omega_0,-\omega_0+\omega)\propto\chi^{(1)}(\omega)\chi^{(1)}(\omega_0)\chi^{(1)}(\omega_0-\omega). \tag{26}$$

So that in the THz region, $\chi^{(2)}(\omega)\propto[\epsilon(\omega)-1]$.

Notes

1. Laser absorption can easily be taken into account by replacing n_g by $n_g+i\alpha$ in Equations (6) and (20). Here α is the absorption coefficient of the material at the laser wavelength.
2. The analogy is not perfectly exact: Bethe's theory considers the diffraction of a plane wave by a conducting plate with a hole whose size is small compared to the wavelength of the radiation. The boundary conditions in our case are slightly different since the source is not surrounded by a conducting medium. The fields might not fall off as sharply as in Bethe's case.
3. The Fabry–Perot effect has been observed on the THz spectrum in experiments (see for example Bakker *et al*. 1998; Han *et al*. 1998).
4. Values are extrapolated from (Bakker *et al*. 1998); Grischkowsky *et al*. 1990; Ralph *et al*. 1992).

References

Auston, D.H. and K.P. Cheung. Coherent time-domain far-infrared spectroscopy. *J. Opt. Soc. Am. B* **2** 606–612, 1984.

Auston, D.H., K.P. Cheung and P.R. Smith. Picosecond photoconducting Hertzian dipoles. *Appl. Phys. Lett*. **45** 284–286, 1984b.

Bakker, H.J., G.C. Cho, H. Kurz, Q. Wu and X.-C. Zhang. Distortion of terahertz pulses in electro-optic sampling. *J. Opt. Soc. Am. B* **15**, 1795–1801, 1998.

Bass, M., P.A. Franken, J.F. Ward and G. Weinreich. Optical rectification. *Phys. Rev. Lett*. **9**, 446–448, 1962.

Beard, M.C., G.M. Turner and C.A. Schmuttenmaer. Progress towards two dimensional biomedical imaging with THz spectroscopy. *Phys. Med. Biol*. **47** 3841–3846, 2002.

Bethe, H.A. Theory of diffraction by small holes. *Phys. Rev*. **66** 163–182, 1944.

Bonvalet, A., M. Joffre, J.L. Martin and A. Migus. Generation of ultrabroadband femtosecond pulses in the mid-infrared by optical rectification of 15 fs light pulses at 100 MHz repetition rate. *Appl. Phys. Lett*. **67** 2907–2909, 1995.

Boyd, G.D., and M.A. Pollack. Microwave nonlinearities in anisotropic dielectrics and their relation to optical and electro-optical nonlinearities. *Phys. Rev. B* **7** 5345–5359, 1973.

Carr, G.L., M.C. Martin, W.R. McKinney, K. Jordan, G.R. Neil and G.P. Williams. High-power terahertz radiation from relativistic electrons. *Nature* (London) **420** 153–155, 2002.

Côté, D., J.E. Sipe and H.M. van Driel. Simple method for calculating the propagation of terahertz radiation in experimental geometries. *J. Opt. Soc. Am. B* **20** 1374, 2003.

Elsaesser, T. and M. Woerner. Femtosecond infrared spectroscopy of semiconductors and semiconductor nanostructures. *Phys. Rep*. **321** 253–305, 1999.

Gallot, G. and D. Grischkowsky. Electro-optic detection of terahertz radiation. *J. Opt. Soc.Am. B* **16** 1204–1212, 1999.

Gallot, G., J. Zhang, R.W. McGowan, T.-I. Jeon and D. Grischkowsky. Measurements of the THz absorption and dispersion of ZnTe and their relevance to the electro-optic detection of THz radiation. *Appl. Phys. Lett*. **74** 3450–3452, 1999b.

Grischkowsky, D., S. Keiding, M. van Exter and Ch. Fattinger. Far-infrared time-domain spectroscopy with teraherz beams of dielectrics and semiconductors. *J. Opt. Soc. Am. B* **7** 2006–2015, 1990.

Grischkowsky, D. *Sensing with TeraHertz Radiation*, ed. Mittleman D., Springer Verlag, Berlin, 2003. Han, P.Y. and X.-C. Zhang. Coherent broadband midinfrared terahertz beam sensors. *Appl. Phys. Lett.* **73** 3049–3051, 1998.

Huber, R., A. Brodschelm, T. Tauser and A. Leitenstorfer. Generation and field-resolved detection of femtosecond electromagnetic pulses tunable up to 41 THz. *Appl. Phys. Lett.* **76** 3191–3193, 2000.

Huber, R., F. Tauser, A. Brodschelm, M. Bichler, G. Abstreiter and A. Leitenstorfer. How many-particle interactions develop after ultrafast excitation of an e-h plasma. *Nature* **414** 286, 2001.

Jackson, J.D. *Classical Electrodynamics* Wiley, New York, Chapter 7, 1962.

Jeon, T.-I. and D. Grischkowsky. Characterization of optically dense, doped semiconductors by reflection THz time domain spectroscopy. *Appl. Phys. Lett.* **72** 3032–3034, 1998.

Kaindl, R.A., S. Lutgen, M. Woerner, T. Elsaesser, B. Notelmann, V.M. Axt, T. Kuhn, A. Hase and H. Künzel. Ultrafast dephasing of coherent intersubband polarizations in a quasi-two-dimensional electron plasma. *Phys. Rev. Lett.* **80** 3575–3578, 1998.

Kaindl, R.A., F. Eickemeyer, M. Woerner and T. Elsaesser. Broadband phase-matched difference frequency mixing of femtosecond pulses in GaSe: experiment and theory. *Appl. Phys. Lett.* **75** 1060–1062, 1999.

Kaindl, R.A., M.A. Carnahan, D.Hägele, R. Lövenich and D.S. Chemla. Ultrafast terahertz probes of transient conducting and insulating phases in an e-h gas. *Nature* **423** 734, 2003.

Katzenellenbogen, N. and D. Grischkowsky. Electrical characterization to 4 THz of N- and P-type GaAs using time-domain spectroscopy. *Appl. Phys. Lett.* **61** 840–842, 1992.

Lee, Y.-S., T. Meade, V. Perlin, H. Winful, T.B. Norris and A. Galvanauskas. Generation of narrow-band terahertz radiation via optical rectification of femtosecond pulses in periodically poled lithium niobate. *Appl. Phys. Lett.* **76** 2505–2507, 2000.

Leemans, W.P., C.G.R. Geddes, J. Faure, Cs. Tóth, J. van Tilborg, C.B. Schroeder, E. Esarey, G. Fubiani, D. Auerbach, B. Marcelis, M.A. Carnahan, R.A. Kaindl, J. Byrd, and M.C. Martin. Observation of THz emission from a laser-plasma accelerated electron bunch crossing a plasma-vacuum boundary. *Phys. Rev. Lett.* **91** 74802, 2003.

Leitenstorfer, A., S. Hunsche, J. Shah, M.C. Nuss and W.K. Knox. Detectors and sources for ultrabroadband electro-optic sampling: experiments and theory. *Appl. Phys. Lett.* **74** 1516–1518, 1999.

Marple, D.T.F., *J. Appl. Phys.* **25** 539, 1964.

Miller, R.C., *Appl. Phys. Lett.* **5** 17–19, 1964.

Mittleman, D.M., G. Gupta, R. Neelamani, R.G. Baraniuk, J.V. Rudd and M. Kosh. Recent advances in THz imaging. *Appl. Phys. B* **68** 1085–1094, 1999.

Nahata, A., D.H. Auston, T.F. Heinz and C. Wu. Coherent detection of freely propagating terahertz radiation by electro-optic sampling. *Appl. Phys. Lett.* **68** 150–152, 1996.

Ralph, S.E. and D. Grischkowsky. THz spectroscopy and source characterization by optoelectronic interferometry. *Appl. Phys. Lett.* **60** 1070–1072, 1992.

Rice, A., Y. Jin, X.F. Ma, X.-C. Zhang, D. Bliss, J. Larkin and M. Alexander. Terahertz optical rectification from ⟨110⟩ zinc-blende crystals. *Appl. Phys. Lett.* **64** 1324–1326, 1994.

Ruffin, A.B., J. Decker, L. Sanchez-Palencia, L. Le Hors, J.F. Whitaker and T.B. Norris. Time reversal and object reconstruction with single-cycle pulses. *Opt. Lett.* **26** 681–683, 2001.

Valdmanis, J. A., G. Mourou and C.W. Gabel. Picosecond electro-optic system. *Appl. Phys. Lett.* **41** 211–212, 1982.

Vodopyanov, K.L. and L.A. Kulevskii. New dispersion relationships for GaSe in the 0.65–18 μm spectral region. *Opt. Comm.* **118** 375–358, 1995.

Williams, G.P. FAR-IR/THz radiation from the Jefferson Laboratory, energy recovered linac, free electron laser. *Rev. Sci. Inst.* **73** 1461–1463, 2002.

Wu, Q., and X.-C. Zhang. Free-space electro-optic sampling of terahertz beams. *Appl. Phys. Lett.* **67** 3523–3525, 1995.

Wu, Q., T.D. Hewitt and X.-C. Zhang. Two dimensional electro-optic imaging of THz beams. *Appl. Phys. Lett.* **69** 1026–1028, 1996.

Xu, L., X.-C. Zhang and D.H. Auston. Terahertz beam generation by femtosecond optical pulses in electro-optic materials. *Appl. Phys. Lett.* **61** 1784–1786, 1992.

Xu, J.Z. and X.-C. Zhang. Optical rectification in an area with a diameter comparable to or smaller than the center wavelength of terahertz radiation. *Opt. Lett.* **27** 1067–1069, 2002.

Zhang, X.-C., X.F. Ma, Y. Jin and T.-M. Lu. Terahertz optical rectification from a nonlinear organic crystal. *Appl. Phys. Lett.* **61** 3080–3082, 1992.